International Journal of Infrared and Millimeter Waves, Vol. 22, No. 11, November 2001 (© 2001)

EUROPEAN MINOR CONSTITUENT RADIOMETER: A NEW MILLIMETER WAVE RECEIVER FOR ATMOSPHERIC RESEARCH

D. Maier,[1,*] N. Kämpfer,[1] J. de la Noë,[2] W. Amacher,[1] A. Barcia,[3] P. Baron,[2] B. Barry,[4] G. Beaudin,[5] J. Cernicharo,[3] B. Ellison,[6] J.-D. Gallego,[3] M. Gustafsson,[7] A. Karpov,[8] U. Klein,[4] K. Künzi,[4] J. Louhi,[7] J. Mallat,[7] D. Matheson,[6] J.-R. Pardo,[5] R. Peter,[1] A.V. Räisänen,[7] P. Ricaud,[2] R. Siddans,[6] C. Viguerie,[5] and M. Wüthrich[1]

[1]*Institute of Applied Physics, University of Berne, Berne, Switzelrand*
[2]*Observatoire de Bordeaux, Floirac, France*
[3]*Centro Astronómico de Yebes, Guadalajara, Spain*
[4]*Institute of Environmental Physics and Remote Sensing University of Bremen, Bremen, Germany*
[5]*Observatoire de Paris, Paris, France*
[6]*Rutherford Appleton Laboratory, Chilton, United Kingdom*
[7]*Helsinki University of Technology, Helsinki, Finland*
[8]*Institut de Radio Astronomie Millimétrique, Saint Martin d'Hères, France*

Received July 25, 2001

Abstract

EMCOR is a heterodyne receiver for the frequency range of 201 to 210 GHz. It has been designed for ground-based measurements of various minor constituents of the stratosphere involved in ozone chemistry. Since the aim was the detection of faint spectral lines, a superconducting tunnel junction has been chosen as mixer element and special care has been taken in developing the calibration unit of the system. The front-end is completed by a quasi-optical system, a solid state local oscillator with electronic tuning and a HEMT pre-amplifier. In the back-end an acousto-optical spectrometer is employed to analyse the signal. A PC controls the whole system. The instrument has been installed at a high mountain site in the Swiss Alps.

Keywords: Millimeter wave receiver, calibration, stratospheric trace gases

*Present address: Institut de Radio Astronomie Millimétrique (IRAM), 300 rue de la piscine, 38406 Saint Martin d'Hères, France

0195-9271/01/1100-1555$19.50/0

1 Introduction

EMCOR (European Minor COnstituent Radiometer) was initiated as a joint project between seven European laboratories with the objective to design and construct a sensitive heterodyne receiver for ground-based measurements of the atmosphere. Its purpose is to detect rotational transitions of molecules involved in the stratospheric ozone depletion phenomenon. Therefore EMCOR should not only work at a fixed frequency, but over a frequency band of several GHz. And since ClO is a key molecule in the process of ozone destruction, this frequency range should contain a ClO line complex. After a spectroscopic study evaluating the different possible frequency bands centred around ClO lines [1, 2] the range of 201 to 210 GHz has been chosen. The modeled spectrum presented in Fig. 1 shows that this frequency range contains besides the required ClO line complex

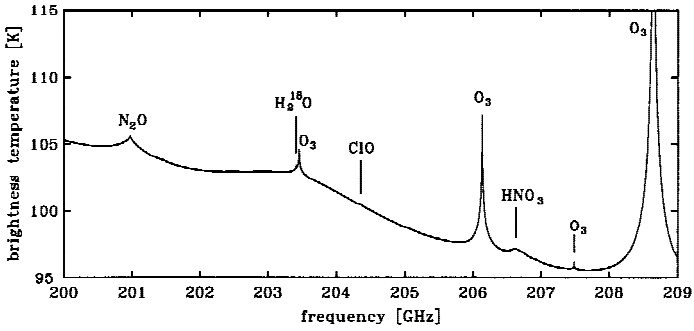

Figure 1: Spring model spectrum calculated for an observation altitude of 3580 m a.s.l. and an elevation angle of 12°.

centered around 204.35 GHz other molecules, as e.g. $H_2^{18}O$, N_2O, or HNO_3, which play a key role in both dynamical and chemical processes occuring in the stratosphere.

The project started in spring 1996. After definition and construction of the subsystems the instrument has been integrated and tested at the University of Berne and finally installed at a high mountain site in the Swiss Alps.

2 Instrument

An overall view of the system is presented in Fig. 2. A rotating mirror at the input of the instrument allows to switch between the atmosphere and the different calibration loads. The signal then passes through the quasi optics and is focussed together with the local oscillator (LO) signal onto the mixer element consisting of a Superconductor-Insulator-Superconductor (SIS) junction. This superconducting tunnel junction is cooled together with the HEMT amplifier in a LHe cryostat. After the low-noise amplifier the intermediate frequency (IF) signal is further processed in the IF chain and finally analysed with an acousto-optical spectrometer. A PC controls observation procedures and data acquisition.

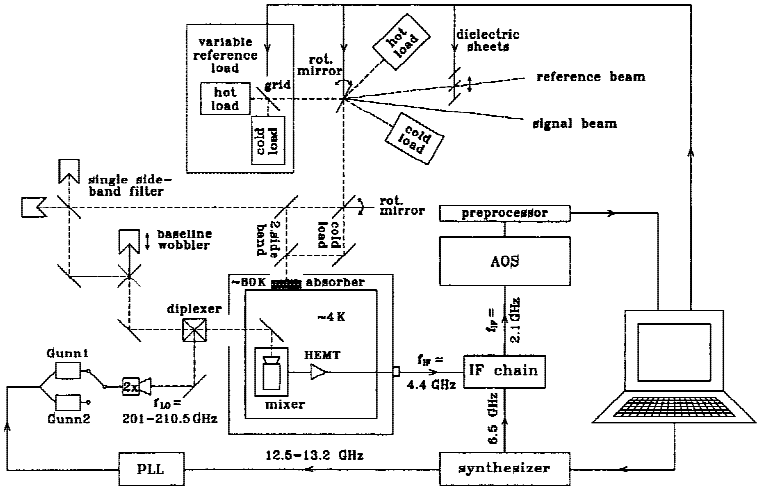

Figure 2: Overall view of the system.

2.1 Quasi optics

The main purpose of the quasi optical system is to focus the incoming beam together with the LO signal onto the mixer element. For the focussing of the beam ellipsoidal mirrors have been preferred to lenses in order to avoid standing waves caused by reflections at the lens surfaces. Other optical components are wire grids, plane mirrors and roof-top mirrors. A schematic view of the quasi optical system is shown in Fig. 3. Apart from the ellipsoidal mirror E0 and the internal cold load which are located inside the cryostat all components are mounted on two optical plates.

A rotating mirror at the input of the quasi optical system allows to switch between the signal passed by the calibration unit, i.e. the atmospheric signal or a signal from one of the calibration loads, and the internal cold load, which is a pyramidally shaped and absorber paint coated copper mounted on the first stage of the closed cycle refrigerator at about 80 K.

All heterodyne receivers are sensitive to two frequency bands, the signal sideband and the image sideband. The unwanted sideband is suppressed employing a Martin-Puplett interferometer. This single sideband (SSB) filter consists of an input polarizer (G3), two roof top mirrors and a wire grid (G2). The incoming beam with the polarization defined by the input polarizer is separated into the two sidebands with orthogonal polarizations. The mixer is only sensitive to one polarization and so only one sideband is received. But the mixer also sees the image sideband reflected at the input polarizer and this contributes to the system noise. In order to keep this contribution as low as possible the image sideband is lead to a cold termination consisting of the internal cold load.

Reflections in the quasi optical system leading to standing waves between the different components are a common problem in millimetre wave radiometry. The receiver then acts like a Fabry-Pérot interferometer and the measured spectra are superimposed by sine waves. A reduction of these artefacts can be achieved by geometrically modulating the optical path length of these parasitic resonators. For this purpose a baseline wobbler

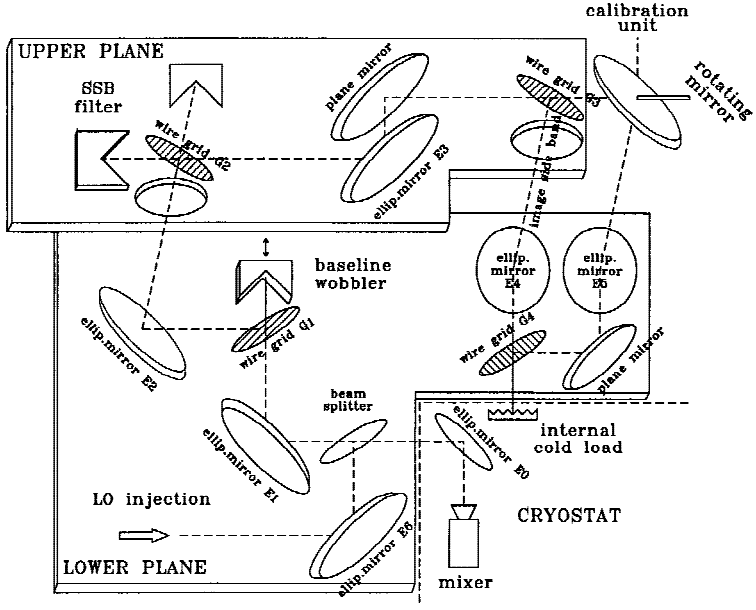

Figure 3: Schematic view of the quasi optics.

has been installed. It consists of a wire grid (G1) and a roof top mirror mounted on a linearly movable unit. The incoming radiation is reflected at the grid to the roof top mirror, where it is re-reflected with rotated polarization and then passes through the grid. The path length modulation is achieved by moving the mirror back and forth sinusoidally with a dc motor. The amplitude of the modulation, of which the optimum value depends on the observation frequency [3], can be adjusted by two excenters mounted on the motor axis.

The LO signal is coupled optically to the signal using a thin mylar foil serving as a beam splitter. The foil is inserted at an angle of 45° in such a way into the beam that the weak atmospheric signal passes almost unaffected through the foil whereas the strong LO signal injected onto the other side of the foil is reflected to a small percentage into the mixer.

Since the optics of the EMCOR instrument have to work correctly over the whole frequency range, the ellipsoidal mirrors E2 and E3 have been fabricated and installed in such a way that they act as a Gaussian telescope [4]. This technique provides beam waists and locations before and behind this mirror pair independent of frequency. So the beam waist at the input of the quasi optics located at the wire grid G3 is 16.5 mm for all frequencies resulting in a beam width of 1.86–1.95° (FWHM) over the frequency range of 201 to 210 GHz. The beam waist between the two mirrors E2 and E3 varies with frequency, but it is always located on the wire grid thus assuring a proper operation of the SSB filter.

2.2 Local oscillator system

The detection of spectral lines requires an LO with a high frequency stability. This is usually achieved by phase-locking a Gunn oscillator to a stable low frequency source and then multiplying the signal. For the EMCOR LO system two varactor-tuned Gunn oscillators covering each a frequency range from 100.5 to 103.0 GHz and from 102.75 to 105.25 GHz are employed [5]. The oscillator appropriate for the measurement is selected with a manual switch. The oscillator signals are frequency stabilized by a phase-locked loop using a reference frequency generated by a synthesizer providing a frequency range of 12.5 to 13.2 GHz. The achieved frequency stability is better than 100 kHz. The

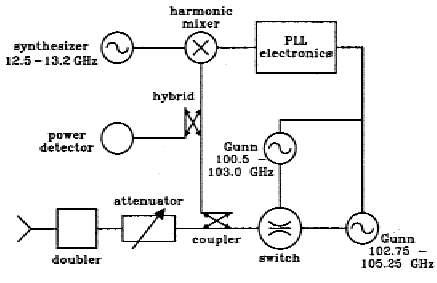

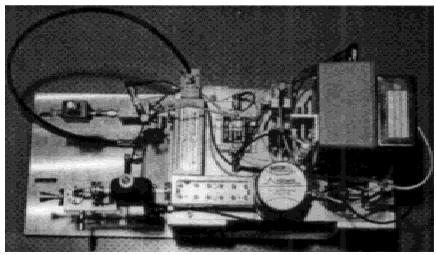

Figure 4: Block diagram and photo of the LO system.

synthesizer output frequency controls the output frequency of the whole LO system. It can be set via the PC with steps of 3.125 MHz resulting in a frequency step of 50 MHz for the LO system. The oscillator signals are multiplied with a doubler and fed into the quasi optics via a Pickett horn antenna adapted to the quasi optics and achieving a coupling of 98–99.8 % over the whole frequency range. The output power level tunable with a manual attenuator is more than −15 dBm over the whole frequency range. Figure 4 shows a block diagram and a photo of the LO system.

2.3 Cryogenic system

In order to cool the superconducting tunnel junction to its operational temperature of about 4 K a cryogenic system had to be installed. This system has been custom-made for the EMCOR instrument by the Rutherford Appleton Laboratory (RAL). Figure 5 shows a drawing as well as a photo of the cryostat in its upright, i.e. normal operation, position. The design uses a 10 l-liquid helium reservoir in combination with a CTI Cryogenics 350 closed cycle refrigerator. The cold head is mounted on an anti-vibration unit that mechanically isolates the cold head from the outer body of the cryostat. The first and second stage of the closed cycle cooler are attached to two separate aluminium radiation shields which surround the liquid helium reservoir. Thus reservoir and cold head together provide three cold surfaces at about 4, 20, and 80 K, onto which components can be attached and cooled. Additionally, the radiation shields reduce the evaporation rate of liquid helium resulting in a hold time of the cryogenic system of about a month.

The 4 K cold stage is constituted by the bottom of the liquid helium reservoir which can be accessed by removal of the square base of the cryostat as well as the first and second stage radiation shield lids. Figure 6 presents a view on the 4 K cold stage of the opened cryostat.

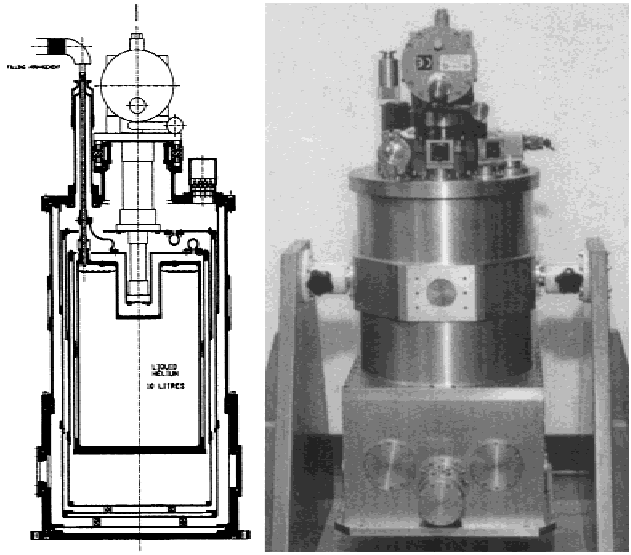

Figure 5: Drawing (left) and photo (right) of the cryostat.

2.4 Mixer element

In order to obtain a receiver with a high sensitivity an SIS tunnel junction has been chosen as mixer element. These junctions are made out of a Nb-Al/AlO_x-Nb trilayer sputtered onto a fused quartz substrate. The junctions are integrated into a Nb matching circuit. This tuning circuit consists of a microstrip line terminated by a 90° radial stub and provides an inductance in parallel to the junction to compensate for its capacitance at the operation frequency. An RF filter consisting of a microstrip line with high and low impedance sections has been integrated on the substrate. The matching circuit has been designed for a frequency range of 201 to 210 GHz.

2.5 Mixer block

The purposes of the mixer block are to provide an appropriate mounting structure for the superconducting tunnel junction with optimum RF and IF electrical circuit characteristics as well as an optimum coupling to the quasi optical system.

A photo of the mixer block is shown in Fig. 7. It is made up of three parts: feedhorn, junction, and backshort blocks. The corrugated feedhorn in the feedhorn block constitutes the transition between the quasi optical system and the mixer input waveguide. It has been designed to match the requirements of the quasi optics. Its circular output waveguide is converted to a reduced height rectangular cross-section via a circular to rectangular waveguide impedance transformer located in the junction block. This block also contains a small filter channel into which the SIS junction is placed and a low frequency IF matching circuit that provides a suitable impedance transformation between the IF output impedance of the junction and the nominal 50 Ω input impedance of the low noise amplifier. Integral with the matching circuit is a junction dc bias input and

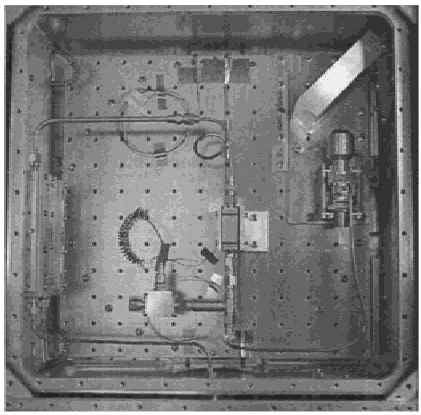

Figure 6: View on the 4 K stage of the opened cryostat.

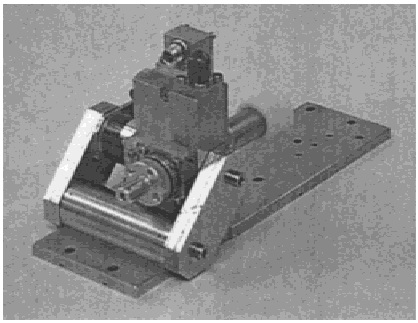

Figure 7: Photo of the mixer block.

sense port.

Since the junction properties as capacitance and normal state resistance vary between fabricated batches a certain degree of tunability is required. This is realized by the use of a tunable backshort which is a movable metal shim placed in a short length of waveguide behind the detecting element and acting as an electrical short.

In order to have the possibility to suppress the Josephson current of the junction a superconducting magnet consisting of over 3000 turns of NbTi wire on a copper bobbin and a flux concentrating yoke have been manufactured and integrated with the mixer block as can be seen on the photo in Fig. 7.

Mixer block, superconducting magnet and first focussing mirror of the quasi optics are integrated onto a common sub-plate assembly that can easily be mounted on the 4 K cold plate of the cryogenic system (see Fig. 6).

Due to temporary difficulties of the Paris Observatory, which was in charge of the junction fabrication, the appropriate SIS junction is not yet available and the EMCOR mixer block can not yet be employed. However, first tests of the system are currently carried out with a 200 GHz mixer kindly provided by the Institute of Radioastronomy at Millimeter wavelengths (IRAM), Grenoble, France.

2.6 Low noise amplifier

The mixer block is immediately followed by an ultra-low noise cryogenically cooled HEMT amplifier used as the first stage of the IF chain. This amplifier has been designed and optimized for a frequency range of 3.9 to 4.9 GHz [6]. In this frequency range and at 15 K an average noise temperature of 7.1 K and a gain of (40.4 ± 0.6) dB have been measured. The amplifier is mounted on the 20 K stage. It can be seen on the left-hand side of the photo shown in Fig. 6. An isolator mounted on the 4 K surface is used at the input of the HEMT amplifier to improve the input match.

2.7 IF chain

In the IF chain [5] the IF signal is further processed to meet the input requirements of the spectrometer, which are a centre frequency of 2.1 GHz and a power level of -5 dBm. A block diagram of the IF chain is presented in Fig. 8. A mixer is used to down-convert the signal from the 3.9–4.9 GHz to the 1.6–2.6 GHz band. The necessary LO signal at 6.5 GHz is generated by a synthesizer. Altogether three amplifiers are employed to achieve the required 50 dB gain: one at 4.4 GHz before the mixer and two at 2.1 GHz. A fourth

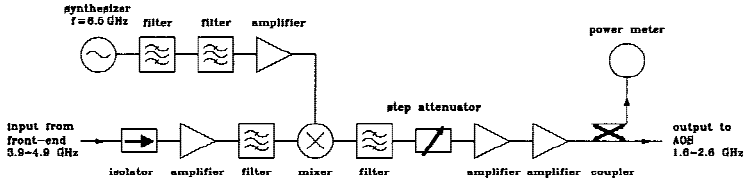

Figure 8: Block diagram of the IF chain.

amplifier amplifies the LO signal at 6.5 GHz. Unwanted harmonic signals are filtered before and after the mixer. Two additional filters in the LO path suppress spurious signals in the LO signal. The isolator at the input of the IF chain avoids reflections which could cause standing waves in the cable between the HEMT and IF chain. The measured gain flatness of the IF chain is 2 dB over the 1 GHz bandwidth.

2.8 Acousto-optical spectrometer and preprocessor

The amplified IF signal is finally analysed using an AOS with 1725 channels and a bandwidth of 1 GHz manufactured by the Observatoire de Meudon.

Data at the output is pre-integrated by a preprocessor, which constitutes the interface between the AOS and the PC. The number of scans to be pre-integrated can be chosen between 1 and 4096. The time required for one scan and thus the minimum integration time is 11 msec. Data is transferred to the PC via an 8 bit digital I/O interface.

2.9 Data acquisition and system control

The whole system is controlled by a PC. Software allowing control of the observation procedures, data acquisition, and real-time monitoring of the observations has been developed using LabWindows/CVI. Raw data is regularly transferred to the University of Berne, where calibration and data reduction are performed. An Internet connection at the observatory allows additionally to monitor the operation of the system from Berne.

3 Calibration

Since the aim of EMCOR is the measurement of faint spectral lines, it has been designed as a balanced radiometer. Nevertheless, stronger lines in the considered frequency range, as e.g. the O_3-line at 208.64 GHz, can be measured in a total power mode. Different balancing methods exist, each having advantages and disadvantages. In order to be able to employ the most suitable technique according to the atmospheric conditions and the

observed molecule, three balancing methods have been installed: a beam switch technique with an atmospheric reference signal, a beam switch technique with a variable reference load and a frequency switch technique. Apart from choosing the most suitable technique on each occasion, EMCOR allows in addition a comparison of the different methods.

3.1 Beam switching with an atmospheric reference signal

In a typical beam switch radiometer as described by Parrish et al. [7] the reference consists of the atmospheric signal measured at a high elevation angle as shown in Fig. 9. Since the path Δz through the atmosphere is much longer for the signal beam resulting in a higher continuum contribution, the continuum contribution of the reference is approximately adapted to that of the signal by inserting a lossy dielectric sheet (D) into the reference beam. Fine-adjustment of the two signals is achieved by adjusting the observation angle ϑ_{sig}. A rotating mirror (RM) switches between the signal beam at a low elevation angle and the reference beam at nearly zenith angle. Due to the conditions at the observatory this high elevation angle can only be achieved by the use of an external mirror (EM) mounted outside the building.

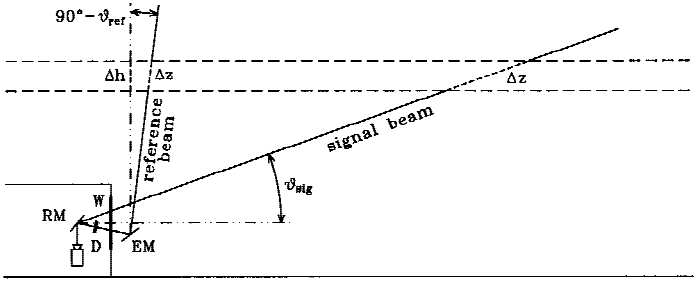

Figure 9: Experimental set-up of the beam switch technique with an atmospheric reference signal. W: window, D: dielectric, RM: rotating mirror, EM: external mirror.

A drawback of this technique is constituted by the adjustment of the observation angle. This might be a problem especially for the detection of faint spectral lines, where the measurements have to be integrated over a long time to achieve a sufficiently good signal-to-noise ratio. In this case the final spectrum consists of a summation over measurements carried out at different observation angles which complicates the retrieval of the altitude profile.

In order to reduce the variation of the observation angle, EMCOR uses several dielectric sheets with different opacities. The angle range has been chosen to be between 10 and 20°. The number of dielectrics and the opacities needed to confine the observation angle to this range has been estimated using a one-layer tropospheric model. According to Fig. 9 the continuum contributions of the signal and the reference beams are

$$\begin{aligned} T_{sig} &= T_{atm}(1-e^{-A_{sig}\tau_z})e^{-\tau_w} + T_w(1-e^{-\tau_w}) \\ T_{ref} &= [T_{atm}(1-e^{-A_{ref}\tau_z})e^{-\tau_w} + T_w(1-e^{-\tau_w})]e^{-\tau_d} \\ &\quad + T_d(1-e^{-\tau_d}), \end{aligned}$$

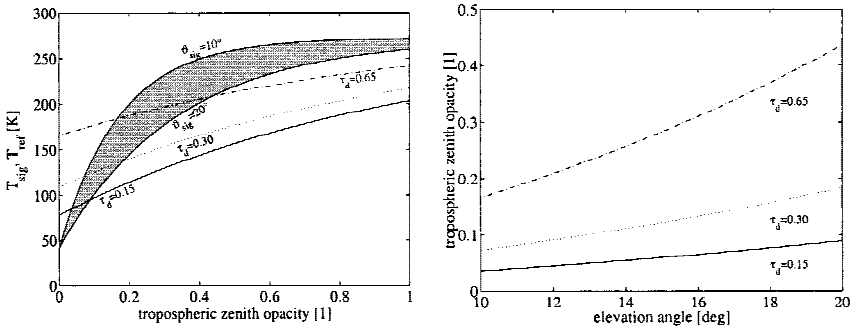

Figure 10: Left: Continuum contributions of signal and reference beams (see text for details). Right: Tropospheric zenith opacities covered by three dielectric sheets.

where T_{atm} is the mean temperature of the troposphere, τ_z is the atmospheric zenith opacity, and T_w, T_d, τ_w and τ_d are the temperatures and opacities of the window and the dielectric sheet. A_{sig} and A_{ref} are the airmass factors in signal beam and reference beam directions given by $A = \Delta h/\Delta z$ with Δh and Δz as defined in Fig. 9. A has been approximated by $A = 1/\sin\theta$ thus neglecting the curvature of the earth. The continuum contributions of signal and reference beams have been calculated as a function of the tropospheric zenith opacity for $\vartheta_{sig} = 10 - 20°$ and $\vartheta_{ref} = 84°$ assuming $T_{atm} = 270$ K, $T_w = 285$ K, $T_d = 300$ K and $\tau_w = 0.16$. The result is shown in Fig. 10 on the lefthand side. The shaded zone indicates the continuum contribution of the signal beam for observation angles between 10 (upper limit) and 20° (lower limit). The continuum contributions of the reference beam for the three dielectric opacities $\tau_d = 0.15, 0.3$, and 0.65 are represented by the three lines. Where one of these curves crosses the shaded zone, balancing is possible with a dielectric of corresponding opacity and an elevation angle between 10 and 20°. According to this analysis the three chosen dielectric opacities of $\tau_d = 0.15$, 0.3, and 0.65 should be sufficient to cover tropospheric zenith opacities up to 0.4 with keeping the observation angle between 10 and 20°. For $T_{sig} = T_{ref}$ and a given dielectric with opacity τ_d the tropospheric zenith opacity can be expressed as a function of the elevation angle. This is shown in the plot on the righthand side in Fig. 10 for the three chosen dielectric opacities. Since the derived opacities are based on a one-layer tropospheric model and several assumptions for the temperatures of the atmosphere, the window and the dielectrics, they only represent estimations for the optimum values, which then have to be adapted by testing at the observation site. As a first try three plexiglas sheets with thicknesses of 1.4, 2.15, and 5.5 mm have been chosen.

Another drawback of this technique is constituted by the line contribution present in the reference beam. Since the difference between signal and reference is evaluated, this line contribution usually leads to an underestimation of the signal.

3.2 Beam switching with a variable reference load

As a second reference a variable reference load [8] has been installed. It consists of a hot and a cold load complemented by a polarizing grid as shown in Fig. 11. The grid is mounted at an angle of 45° with respect to the optical axes, so that the receiver sees the signal of the cold load reflected at the grid and the transmitted signal of the hot load. Since the receiver is only sensitive to one polarization, the contributions of the two loads

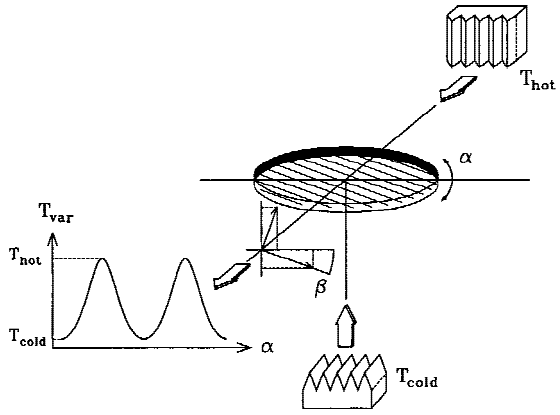

Figure 11: Schematic view of the variable reference load.

to the received signal T_{var} can be varied by rotating the grid. If the receiver is sensitive to the horizontal polarization, the signal seen by the mixer is given by

$$T_{var} = T_{cold} \cos^2 \beta + T_{hot} \sin^2 \beta, \tag{1}$$

where β is the angle between the wires as seen in the direction of signal propagation along the optical axis and the horizontal axis. The signal can also be expressed as a function of the grid angle, which is measured in the grid plane with $\alpha = 0°$ for horizontal wires,

$$T_{var} = \frac{2\,T_{cold} + T_{hot} \tan^2 \alpha}{2 + \tan^2 \alpha}. \tag{2}$$

These equations show that the signal can be tuned to any value between T_{hot} and T_{cold}. In particular, it can not be tuned to a value below T_{cold}, which means for EMCOR below about 77 K. But at the observation site the measured brightness temperatures in this frequency range can be as low as 50 K. During these good weather periods balancing with the variable reference load is no longer possible and one of the other balancing methods has to be employed.

3.3 Frequency switching

In case of the frequency switching the reference consists of the atmospheric reference shifted in frequency. This is realized by shifting the LO frequency. This frequency shift is typically in the order of a few MHz. The major drawback of this method is the limitation of the frequency shift by the requirement of a constant gain for the different frequencies, so that only very narrow lines can be observed.

3.4 Experimental setup

Figure 12 shows the experimental setup of the two beam switch techniques. With the rotating mirror M the beam is reflected into the quasi optics. The mirror can be switched

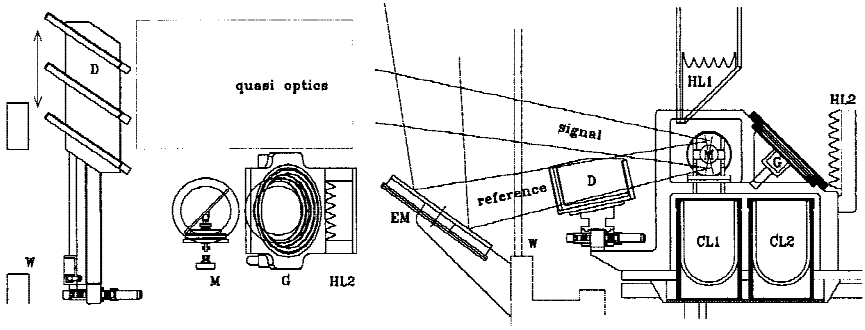

Figure 12: Schematic view of the calibration unit seen from above (left) and in a side view (right). W: window, D: dielectrics, M: rotating mirror, EM: external mirror, CL1,2: cold loads, HL1,2: hot loads, G: polarizing grid.

between five positions: hot load, cold load, atmospheric signal, atmospheric reference and variable reference.

The atmospheric signal is measured at an elevation angle between 10 and 20°. The angle can be set by the PC which allows for its adjustment when employing the beam switch technique with the atmospheric reference.

For the atmospheric reference the mirror looks at −12°. The beam passes through the dielectric sheet D and the window W and is then reflected at the external mirror in 6° zenith direction. In order to avoid icing up, which is a problem at an altitude of 3580 m the mirror is continously heated to a temperature of about 300 K. The three dielectrics with different opacities used to adjust for different atmospheric conditions are mounted on a linearly movable unit which can be controlled via the PC. According to the atmospheric condition the most suitable dielectric is automatically chosen and moved at Brewster's angle into the beam.

The hot load HL1 consisting of an absorber in a temperature stabilized box, set to 313 K, and the cold load CL1 with another absorber immersed in liquid nitrogen are used for absolute gain calibration.

A second pair of hot and cold loads, HL2 and CL2, are needed for the variable reference load. Here the hot load is just an absorber at room temperature. The polarizing grid G can be rotated with a PC controlled motor via a gear.

4 System integration and tests

After definition and construction of the subsystems the instrument has been integrated and tested at the University of Berne and finally installed at the International Scientific Station Jungfraujoch (ISSJ) at an altitude of 3580 m a.s.l. in the Swiss Alps. Further tests have been carried out at the observation site.

A photo of the instrument at the observatory is shown in Fig. 13. The system is installed inside the laboratory and the beam passes through a microwave window. In the beginning a polyethylene window has been used. Later on it has been changed to styrofoam.

The whole frontend is mounted on a movable support, which is adjusted with respect

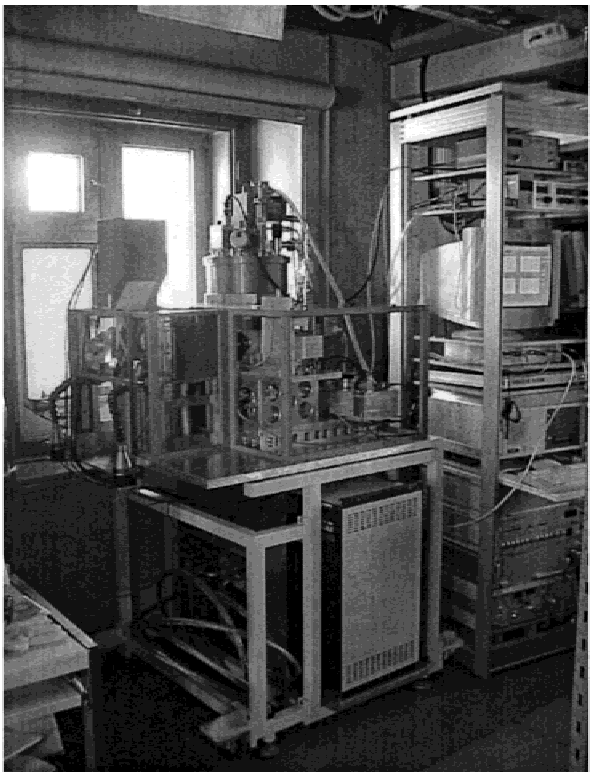

Figure 13: Instrument installed at the ISSJ.

to the external mirror mounted outside on the wall of the building. Backend, electronics and PC are installed in a rack. In order to protect critical components such as the superconducting tunnel junction from damage due to power failures, an uninterruptable power supply has been installed. It is mounted onto the support under the frontend and can be seen on the photo in Fig. 13 in the front. The compressor of the closed cycle refrigerator is also placed under the frontend. But in order to avoid perturbations of the measurement due to its vibrations, it is placed on a separate movable support.

4.1 Single sideband filter

In order to determine the optimum positions of the SSB filter for the different observation frequencies the transmission of signal and image sidebands have been measured for each measurement setup. The signals were generated employing a Gunn oscillator combined with a doubler. The suppressions of the image sideband achieved for the different molecules are summed up in the table presented in Fig. 15. As an example of the measurements the normalized transmissions of signal and image sidebands as obtained for the ClO frequency are shown in Fig. 14.

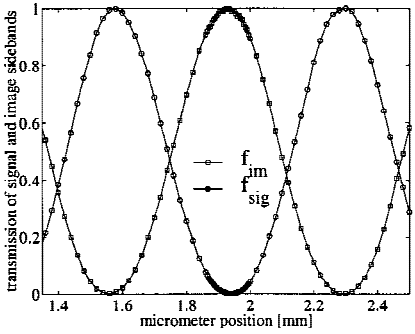

Figure 14: Normalized transmissions of signal (□) and image (○) sidebands for the ClO frequency.

molecule	f [GHz]	SB	P/P_{max} [dB]
ClO	204.35	LS	28.4
N_2O	200.96	LS	29.7
$H_2^{18}O$	203.41	LS	27.8
HNO_3	206.62	US	25.1
O_3	208.64	US	28

Figure 15: Achieved suppression for the different observation frequencies. (SB: sideband, US: upper sideband, LS: lower sideband.)

4.2 Standing waves

In order to reduce the effects of standing waves a baseline wobbler has been integrated within the quasi optical system. The amplitude of its back and forth motion has been optimized with regard to the ClO observation frequency. However, since the optimum value only changes within a few percent over the whole frequency range, the results achieved for the different observation frequencies are quite similar. Figure 16 shows an example of its operation. The two curves show an SSB measurement of a load at room temperature carried out at the ClO observation frequency. The dashed curve represents the measurement without baseline wobbler. The spectrum is clearly superimposed by sine waves with amplitudes up to a few K due to reflections within the system. A wave with about 16 periods over the bandwidth can be clearly distinguished. This corresponds to a period of about 63 MHz. From this period the distance between the reflecting components can be calculated with

$$L = \frac{c}{2P}, \tag{3}$$

where c denotes the velocity of light and P is the period of the sine wave, giving a distance of approximately 2.5 m. This corresponds to the distance between the mixer and one of the loads, so that this sine wave is due to a reflection at the loads. The solid line in Fig. 16 shows the same measurement carried out with phase modulator. It can be seen that the wobbler suppresses the effects of standing waves by about 10 dB reducing the amplitude to a few tenth of a Kelvin. This is not yet optimal for the measurement of faint spectral lines, but if the standing waves are stable with time, their effects on the measurement are further reduced by the balancing technique.

The phase modulator can only reduce standing waves when it is located within the optical path between the reflecting components. Therefore reflections between successive components are not affected by the phase modulator. Since the distance between successive components is usually quite short, such reflections reveal themselves as long-period superimposed sine waves in the spectra.

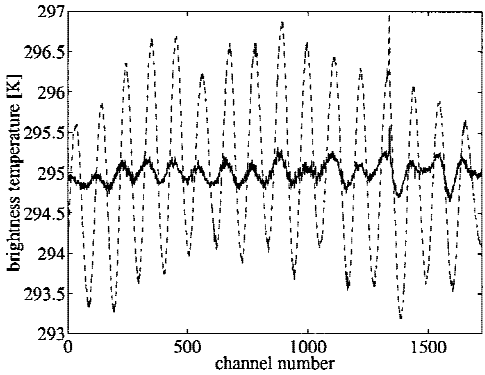

Figure 16: Measurement of a load at room temperature without (- -) and with (–) baseline wobbler.

4.2.1 Cold load reflections

The most difficult standing waves are those who are not stable, i.e. where the distance between the reflecting components changes with time. If the distance is quite long resulting in a superimposed sine wave with a period much shorter than the bandwidth, then the broad band signal remains stable and the artefacts in the spectra might be cancelled out by integrating over some time. But if the superimposed sine wave has a period comparable to the bandwidth, which corresponds in our case to a distance of 15 cm, the broad band signal will oscillate with time. Figure 17 shows an example of such an effect. The black line in the plot on the lefthand side shows the variation of the cold load signal under normal observation conditions. It clearly oscillates with a period around 5 min. For comparison the variation of the hot load is represented by the dotted line. Since the hot load signal is stable within a percent, the oscillation cannot be caused by system effects, but must be due to a change in the cold load itself. It is most probably caused by the evaporation of liquid nitrogen. The evaporation rate has been measured to be approximately 2 cm/h giving rise to a change in distance of about 13 wavelengths per hour. This is in good agreement with the observed period of 5 min. This oscillation is probably caused by a reflection between the absorber material immersed in liquid nitrogen and the nitrogen surface. Since this distance is around 15–20 cm, it causes the spectrum to be superimposed by a sine wave with period of 0.75 to 1 GHz. When now the distance slightly diminishes, not only the period but also the phase of this sine wave changes and it moves through the spectrum resulting in an oscillation of the broadband signal. Since this reflection is not affected by the baseline wobbler, it has a quite large amplitude of $\pm 5\%$.

Since the cold load signal is used as calibration signal this effect constitutes a severe problem for the measurement, especially when brightness temperatures close to the cold load temperature and below are measured. As an attempt to reduce standing waves between absorber and liquid nitrogen surface the mirror has been slightly tilted so that the optical path is now no longer perpendicular to the nitrogen surface (see Fig. 12). The plot in Fig. 17 on the righthand side shows the broadband hot (dotted line) and cold (solid line) load signals for this modified setup. The oscillation amplitude is reduced

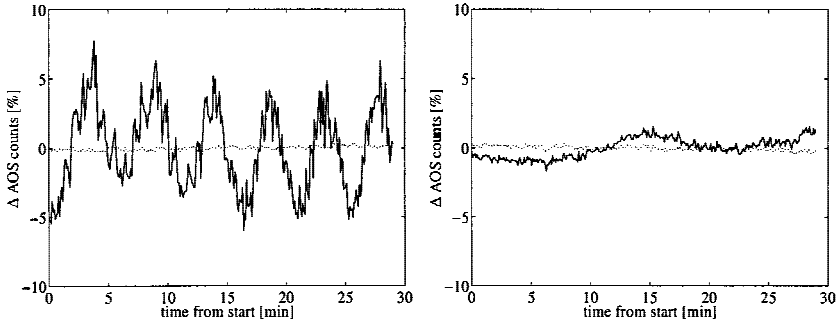

Figure 17: Variation of cold (solid line) and hot (dotted line) load signals. Left: Normal setup. Right: Modified setup.

and the period has changed. Nevertheless, the artefacts in the measurement could not be completely suppressed.

Obviously, this reflection depends very strongly on the load material and its position. Since this is a microwave absorber material immersed in liquid nitrogen, its position is not fixed. Especially when refilling the load with liquid nitrogen the absorber moves thus affecting the quality of the measurement.

4.2.2 Hot load reflections

As discussed in the previous sections reflections at the loads constitute a severe problem for the measurements. Since their effects cannot be completely suppressed by employing a baseline wobbler, the reflection itself should be reduced as far as possible by choosing an absorber material with low reflection. The first material employed for all loads was ECCOSORB CV3 (black). Other materials available at our laboratory were ECCOSORB CV3 (frontface painted white), ECCOSORB CR110, and Keating RAM. In order to determine the most suitable choice for the hot load among these different absorber materials, a rough test was carried out. Each absorber was employed once as hot load measuring the spectrum of an ECCOSORB CV3 (black) at room temperature. The Fourier transform of the four measured spectra has been calculated to determine the periods of the superimposed sine waves present in the measurement. From these periods the distances between the reflecting components have been calculated using equation (3). Figure 18 shows the Fourier transform of the four measurements plotted against distance. The distance from the mixer to the ECCOSORB CV3 (black) and to the hot load are 2.3 and 2.1m, respectively. Reflections at these two absorbers are represented by the corresponding peaks in the plots. For the measurement with the same material as antenna and as hot load the two peaks are approximately equal. This confirms the origin of the two peaks. For ECCOSORB CV3 white and especially for ECCOSORB CR110 the hot load reflection is stronger than the antenna reflection. When Keating RAM is used for the hot load the antenna reflection becomes more important.

From these qualitative experiments we deduced that Keating RAM shows the least reflections at our measurement frequency among the tested materials. Therefore it is now employed for the hot load as well as for the variable reference load.

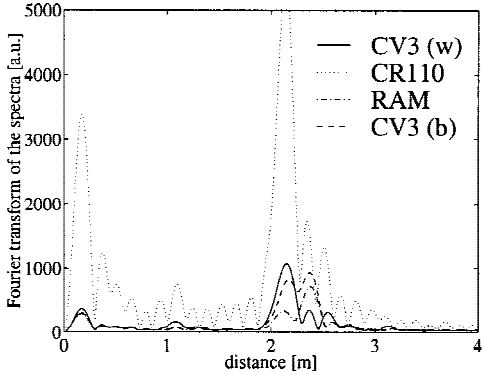

Figure 18: Fourier transform of the four spectra measured with different hot load materials.

4.3 Atmospheric reference

The opacities of the plexiglas sheets have been measured at the observation site. The results were 0.123, 0.182, and 0.535 for the three thicknesses of 1.4, 2.15, and 5.5 mm, respectively. Measurements carried out on one day using the atmospheric reference have been used to evaluate the accuracy of our theoretical approach presented in 3.1. For equal continuum contributions of signal and reference beams the tropospheric zenith opacity can be expressed as a function of the elevation angle as shown in Fig. 10 at the bottom. Since T_{ref} is a function of τ_z, it can also be expressed as a function of the elevation angle. The dots shown in Fig. 19 represent the reference brightness temperature as a function of the elevation angle as measured on September 9, 1998. The solid line shows the

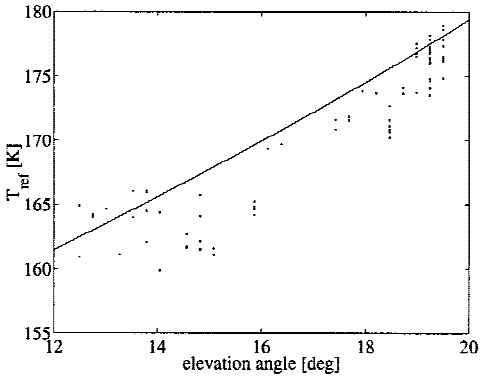

Figure 19: Reference brightness temperature as a function of the elevation angle ϑ_{sig}. Measurement (·) and theory (–).

theoretical result calculated with the mean temperatures of the dielectric and the window measured on this day. T_{atm} has been taken as $\overline{T_{ext}}$ – 12 K [9]. For equal elevation angles the calculated brightness temperatures are higher than the measured ones. Nevertheless, the agreement between theory and experiment seems to be good enough to use the theoretical approach for an evaluation of the needed dielectric opacities. But it has to be taken into account that seasonal temperature changes of the atmosphere as well as at the observatory affect the balancing range of the dielectrics.

A more severe problem is constituted by the changing properties of the dielectric itself. Various measurements of the dielectric opacities carried out over a period of one year revealed that the opacities decreased about 15 % during this period.

4.4 Variable reference load

In order to check the relation given by equation (2) the signal of the variable reference load has been measured as a function of the grid angle α. The brightness temperatures of the hot and the cold loads as well as an angle offset have been fitted to the measurements using equation (2). The result is shown in Fig. 20 at the top. The circles represent the measurement and the fit is given by the solid line. The plot at the bottom shows the difference between measurement and fit revealing a discrepancy of up to 6 K. The difference between measurement and fit for intermediate temperatures is expected and due to the non-linearity of the hot-cold calibration, but it should vanish at the calibration points. In our measurement the respective distances between the maxima and the minimum slightly

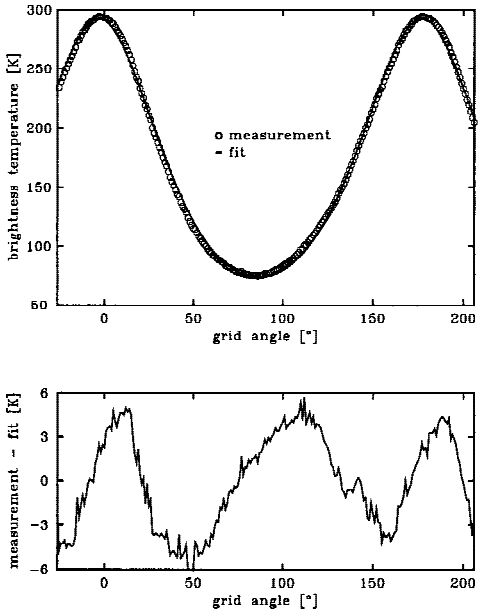

Figure 20: Top: Signal of the variable reference: Measurement (o) and fit (-). Bottom: Difference between measurement and fit.

differ from the theoretical value of 90°. This is probably caused by a non-linearity in the read-out of the grid angle. Because of this effect the positions of the extrema could not be very well fitted resulting in quite large differences between measurement and fit even at the calibration points.

However, the discrepancies of experiment and theory do not affect the quality of the balancing, since only the derivative of the curve described by equation (2) is needed to find the optimum grid position. The difference between the brightness temperatures of the sky and the variable reference load is measured and the grid is adjusted according to

$$d\alpha = dT \cdot \frac{(2\cos\alpha + \tan\alpha \cdot \sin)^2}{4\tan\alpha(T_{hot} - T_{cold})}. \tag{4}$$

5 First measurements

Figure 21 shows as an example the measurement of the $H_2^{18}O$ line at 203.41 GHz. This measurement has been carried out using the variable reference load for balancing. The plot on the lefthand side shows the hot-cold calibrated signals of the atmosphere and the variable reference (without line contribution). The spectra are superimposed by several sine waves due to reflections within the system, so that the $H_2^{18}O$-line located on the wing of the O_3-line at 203.45 GHz is hardly perceptible. One sine wave with a period around 1 GHz can be clearly distinguished. It only appears for sky brightness temperatures around or below the cold load temperature and is probably due to the reflection between the absorber immersed in liquid nitrogen and the nitrogen surface as discussed in 4.2.1. Since this reflection is not affected by the phase modulator, the sine wave has a quite large amplitude of over 1 K.

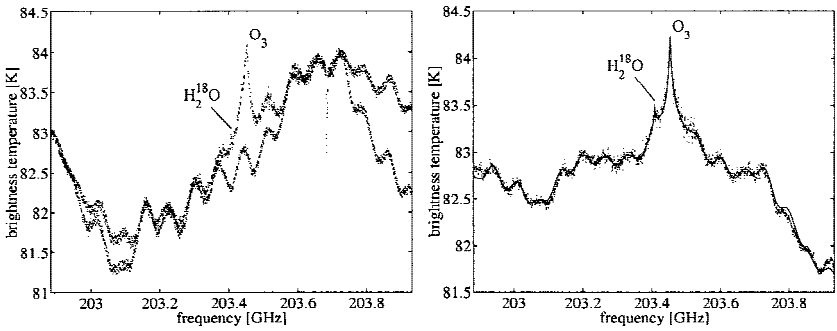

Figure 21: Measurement of the $H_2^{18}O$-line at 203.41 GHz. Left: Total power calibration of signal and reference. Right: Balanced calibration (see text).

The dots in the plot on the righthand side represent the same measurement making use of the balancing concept. The spectrum has been calibrated with

$$T_b = \frac{S - R}{R} \cdot (\overline{T_{ref}} + T_{rec}) + \overline{T_{ref}}, \tag{5}$$

where S and R are the signals of the atmosphere and the reference, respectively, T_{rec} is the receiver noise temperature, and $\overline{T_{ref}}$ is the measured mean brightness temperature

of the variable reference [8]. The superimposed sine waves present in the total power measurement are considerably reduced by the balancing method. The long-period wave is no longer distinguishable and the amplitudes of the short-period waves are reduced. Now the $H_2^{18}O$-line has become visible.

A preliminary retrieval of the altitude profiles has been carried out using the optimal estimation method [10] and employing the technique described in [11] which allows a simultaneous fit of superimposed sine waves. The solid line in Fig. 21 represents the modelled spectrum calculated with the retrieved altitude profiles of O_3 and $H_2^{18}O$ and the fitted amplitude and phase of several sine waves. It can be seen that the residual waves present in the spectrum can be well fitted during the retrieval.

6 Conclusions

A sensitive millimetre wave heterodyne receiver for atmospheric measurements in the frequency range of 201 to 210 GHz has been designed and constructed. In order to be able to measure even very faint spectral lines special efforts have been made to design a suitable calibration unit.

The radiometer has been installed at a high mountain site in the Swiss Alps. First measurements of $H_2^{18}O$ have proven that the system is operational. Nevertheless, further improvement of the system is going on to ensure its operation on a regular basis.

Acknowledgements

The authors would like to thank Prof. H. Debrunner of the Foundation of the Alpine Scientific Stations Jungfraujoch and Gornergrat for the possibility to install the instrument at the Sphinx Observatory. Special thanks go to P. Kuster and H.R. Staub for their support at the observatory. This work was supported by BBW-contract No. 95.0433 as part of EC-contract ENV4-CT95-0137.

References

[1] J. de la Noë, P. Ricaud, P. Baron, G. Beaudin, C. Viguerie, J.-R. Pardo, J. Cernicharo, A. Barcia, J.-D. Gallego, N. Kämpfer, D. Maier, R. Peter, D. Matheson, B. Ellison, R. Siddans, K. Künzi, U. Klein, B. Franke, J. Louhi, M. Gustafsson, J. Mallat, and A. Räisänen, "A European microwave radiometer to measure some stratospheric minor constituents: the emcor instrument," in *Proceedings of the 2nd ESA Workshop on Millimetre Wave Technology and Applications: Antennas, Circuits and Systems*, Millilab, Espoo, Finland, May 1998.

[2] J. de la Noë, P. Ricaud, P. Baron, O. Lezeaux, C. Viguerie, J.-R.Pardo, G. Beaudin, J. Cernicharo, A. Barcia, J.-D. Gallego, D. Maier, R. Peter, N. Kämpfer, W. Amacher, A. Widmer, M. Wüthrich, B. Ellison, D. Matheson, R. Siddans, B. Kerridge, U. Klein, B. Barry, K. Künzi, J. Louhi, M. Gustafsson, J. Mallat, and A. Räisänen", "Development of a European ground-based microwave radiometer to measure stratospheric minor constituents," Final Report to the EC, contract ENV4-CT95-0137, 1999.

[3] J.J. Gustincic, "A quasi-optical receiver design," in *IEEE-MTT-S, International Microwave Symposium Digest*, San Diego, May 1977, pp. 99–100.

[4] P.F. Goldsmith, "Quasi-optical techniques at millimeter and submillimeter wavelengths," in *Infrared and Millimeter Waves vol. 6: Systems and Components*, K.J. Button, Ed., New York, 1982, Academic Press.

[5] J. Louhi, M. Gustafsson, J. Mallat, and A. Räisänen, "Local oscillator and IF chain for European millimeter wave radiometer, EMCOR," Report S229, Helsinki University of Technology, Radio Laboratory, October 1997.

[6] J.D. Gallego, R. Baeza, R. Garcia, and D. Geijo, "Measurements of EMCOR cryogenic 3.9–4.9 GHz HEMT amplifier," Technical report CAY 1997-1, Centro Astronómico de Yebes, May 1997.

[7] A. Parrish, R.L. de Zafra, P.M. Solomon, and J.W. Barrett, "A ground-based technique for millimeter wave spectroscopic observations of trace constituents," *Radio Science*, vol. 23, pp. 106–118, 1988.

[8] R. Krupa, *Millimeterwellen-Radiometrie stratosphärischer Spurengase unter Anwendung balancierter Kalibrierung*, Ph.D. thesis, University of Karlsruhe, 1997.

[9] T. Ingold, R. Peter, and N. Kämpfer, "Weighted mean tropospheric temperature and transmittance determination at millimeter-wave frequencies for ground-based applications," *Radio Science*, vol. 33, pp. 905–918, 1998.

[10] C.D. Rodgers, "Retrieval of atmospheric temperature and composition from remote measurements of thermal radiation," *Rev. Geophys. Space Phys.*, vol. 14, pp. 609–624, 1976.

[11] M. Kuntz, "Retrieval of of ozone mixing ratio profiles from ground-based millimeter wave measurements disturbed by standing waves," *J. Geophys. Res.*, vol. 102, no. D18, pp. 21,965–21,975, 1997.